PAPER

Check for updates

A highly selective "turn-on" water-soluble fluorescent sensor for gallium ion detection†

Pengfei Wang, [iD] [a] Fanda Meng,[b] Hao Su,[a] Lijie Liu,[a] Maroof Ahmad Khan[a] and Hui Li [iD] *[a]

In this work, a novel sensor, (*E*)-*N*′-(3-(*tert*-butyl)-2-hydroxybenzylidene)thiophene-2-carbohydrazide (**1**), based on salicylaldehyde and thiophene hydrazide moieties was designed and synthesized. The single-crystal structure of **1** was achieved and studied for understanding its functional properties. The interaction and recognition abilities of **1** with different metal ions were investigated. Sensor **1** showed excellent "turn-on" fluorescence with highly selective and specific recognition ability in the presence of gallium ions (Ga^{3+}) in an aqueous solution. The sensing behavior of **1** with Ga^{3+} was also studied by photophysical experiments, ESI-MS analysis, and ^{1}H NMR titration. The limit of detection (LOD) and limit of quantification (LOQ) of **1** for the detection of Ga^{3+} in an aqueous solution were calculated as 58 nM, and 192 nM, respectively. DFT calculations were carried out to optimize the configuration of **1** and **1**–Ga^{3+} complexes and rationalize the photophysical experimental data. Highly selective test strips based on sensor **1** were developed for Ga^{3+} detection. Sensor **1** was also used to detect Ga^{3+} in actual water samples, and a considerable recovery rate was obtained.

Introduction

Gallium is a silvery-white rare metal that does not exist in its simple form in nature.[1,2] It exists in trace amounts in bauxite and zinc earth in the form of Ga^{3+} salt.[3] Gallium is employed in the manufacture of many electronic products such as LEDs and solar cells because of its excellent chemical and physical properties.[4–10] Ga^{3+} salt is also used as an anticancer drug because of its excellent biological affinity for tumor tissues.[11–13] Owing to its excellent physical, chemical, and biological applications, the use of Ga^{3+} is gradually increasing, resulting in the gradual accumulation of Ga^{3+} in the environment. Although Ga^{3+} plays a critical role in human life activities, disease problems caused by Ga^{3+} ion exposure cannot be ignored. Long-term exposure to Ga^{3+} can cause numerous side effects to the human body, such as gastrointestinal diseases, anemia, and coma, and may even lead to death.[14,15] However, there are few reports on Ga^{3+} sensors and even fewer reports on fluorescent sensors. To the best of our knowledge, reports on Ga^{3+} fluorescent sensors are rare.[16–28] Among the reported sensors, few work in aqueous solutions. In addition, most reported Ga^{3+} sensors recognize not only Ga^{3+},

but also other interfering ions[29–33] (such as Al^{3+} and In^{3+}) simultaneously, which will interfere with the judgment of detection results. A sensor that can specifically recognize a certain ion will avoid misjudgment in actual use. Fluorescent sensors have the characteristics of high sensitivity, good selectivity, convenient operation, and intuitive observation.[34–44] Therefore, it is necessary to develop a fluorescent sensor that can recognize Ga^{3+} specifically and selectively in an aqueous solution.

Acylhydrazone Schiff bases are widely studied because of their simple synthesis, excellent easy-to-adjust photoelectric properties, multiple coordination sites, and easy combination with metal ions.[45] In recent decades, a large number of Schiff base-based fluorescent sensors have been reported.[45–48] However, most sensors reported are related to identifying common metal ions and heavy metal ions such as aluminum and mercury.[49,50] There are limited reports on the sensors of some trace elements (such as Ga^{3+}). Therefore, it is also significant to study trace element sensors. In the past few years, our group has reported some research in fluorescence detection fields.[51–54] Based on previous research, a novel fluorescent sensor based on acylhydrazone Schiff base was designed and synthesized in this work. It exhibits high selectivity and specificity for fluorescence "turn-on" recognition of Ga^{3+} in an aqueous solution. To study the working mechanism and the internal molecular interaction, we grew a single crystal of sensor **1** and carried out photophysical experiments, ^{1}H NMR titration, and ESI-MS mass spectrometry analysis. DFT calculations were also carried out to study the energy levels of the molecular

[a]Key Laboratory of Cluster Science of Ministry of Education, School of Chemistry and Chemical Engineering, Beijing Institute of Technology, Beijing 100081, P. R. China. E-mail: lihui@bit.edu.cn; Tel: +86-10-81381366

[b]School of Basic Medicine, Shandong First Medical University, Shandong Academy of Medical Sciences, Jinan, 250062, P. R. China

† Electronic supplementary information (ESI) available. CCDC 2064800. For ESI and crystallographic data in CIF or other electronic format see DOI: 10.1039/d1ra02582a

orbitals and the change in the HOMO–LUMO band gaps before and after the coordination process. Moreover, highly selective test strips based on sensor **1** were developed for Ga^{3+} detection. Sensor **1** was also used to detect Ga^{3+} in actual water samples. We expect this work will contribute to the development and application in Ga^{3+} detection fields.

Experimental

Chemicals and solvents

All chemicals and solvents (analytical and spectral) were used as standard and purchased from Sigma-Aldrich.

Measurements and instruments

^1H NMR and ^{13}C NMR spectra were recorded using a Bruker AVANCE III HD 400 MHz nuclear magnetic resonance spectrometer and a Bruker AVANCE III HD 700 MHz nuclear magnetic resonance spectrometer. Absorption spectra were recorded using a PERSEE TU-1950 double-beam UV-vis spectrophotometer at room temperature. Fluorescence emission spectra were recorded using a HITACHI F-7000 fluorescence spectrophotometer. Quantum yield was collected using a QuantaurusQY Absolute PL quantum yield spectrometer, C11347-11|Hamamatsu Photonics. ESI-MS spectra were recorded using a Q-TOF 6520 LC-MS AGILENT instrument. IR spectra were recorded using a Thermo IS5 Fourier transform infrared spectrometer. Elemental analysis was performed using an EA3000 elemental analyzer at the Analysis and Testing Center of Beijing Institute of Technology.

Preparation and characterization of 1

(*E*)-*N*′-(3-(*tert*-Butyl)-2-hydroxybenzylidene)thiophene-2-carbohydrazide (1). A typical synthesis of sensor **1** was performed by refluxing a mixture of 3-(*tert*-butyl)-2-hydroxybenzaldehyde (1.0 mmol) and thiophene-2-carbohydrazide (1.01 mmol) in 10 mL methanol for 24 h. After the reaction was complete, the obtained mixture was cooled to room temperature. The product was filtered off and then washed with cold methanol and cold water. The resulting solid product was obtained in 98% yield as a white powder. ^1H NMR (400 MHz, DMSO-d_6) δ 12.32 (s, 1H), 12.26 (s, 1H), 8.55 (s, 1H), 7.93 (s, 1H), 7.91 (d, J = 0.9 Hz, 1H), 7.31 (s, 1H), 7.29 (s, 1H), 7.28–7.22 (m, 1H), 6.89 (t, J = 7.7 Hz, 1H), 1.40 (s, 9H). ^{13}C NMR (176 MHz, DMSO-d_6) δ 157.43, 156.83, 150.58, 137.17, 136.36, 132.30, 129.52, 129.38, 128.54, 128.21, 118.77, 117.64, 34.46, 29.22. HRMS calcd. $C_{16}H_{18}N_2O_2S$ 302.1089, calcd. $C_{16}H_{19}N_2O_2S^+$ 303.1162, found M + H$^+$ 303.1163. Elemental analysis: calcd for $C_{16}H_{18}N_2O_2S$: C, 63.55; H, 6.00; N, 9.26; O, 10.58; S, 10.60. Found C, 63.49; H, 5.95; N, 9.04; S, 10.46.

UV-vis titration experiments

A solution of sensor **1** (3 mM, dissolved in DMSO) was prepared, and the sensor **1** solution (10 μL, 3 mM in DMSO) was diluted to 2.990 mL bis–tris buffer solution (pH = 7.4) to achieve a final concentration of 10 μM (0.3% DMSO/H_2O). Then, 1–5 μL $Ga(NO_3)_3$ (3 mM) aqueous solution was added to 3 mL above **1** solution. After mixing for 5 minutes, UV-vis absorption spectrum experiments were performed at room temperature.

Fluorescence titration experiments

A solution of sensor **1** (3 mM, dissolved in DMSO) was prepared, and the sensor **1** solution (1 μL, 3 mM in DMSO) was diluted to 2.999 mL bis–tris buffer solution (pH = 7.4) to achieve a final concentration of 1 μM (0.03% DMSO/H_2O). Then, 1–5 μL of 0.3 mM $Ga(NO_3)_3$ aqueous solution was added to 3 mL above **1** solution. After mixing for 5 minutes, fluorescence spectrum experiments were performed at room temperature.

Job's plot measures

First, 0.1 μM sensor **1** bis–tris solution (dissolved in 0.03% DMSO/H_2O) and $Ga(NO_3)_3$ bis–tris solution were prepared respectively. A series of solutions containing **1** and $Ga(NO_3)_3$ were prepared to keep the volume of each solution at 3 mL. The volume ratio of **1** and Ga^{3+} are 10 : 0, 9 : 1, 8 : 2, 7 : 3, 6 : 4, 5 : 5, 4 : 6, 3 : 7, 2 : 8, 1 : 9, and 0 : 10. After mixing for 5 minutes, the fluorescence data were collected at room temperature. Job's plot curve was obtained by plotting the volume ratio of Ga^{3+} ion to **1** + Ga^{3+} ion and the fluorescence intensity on the X and Y axes, respectively.

Competition experiments

A solution of sensor **1** (3 mM, dissolved in DMSO) was prepared, and 1 μL sensor **1** solution (3 mM) was diluted to 2.999 mL bis–tris buffer solution to achieve a final concentration of 1 μM. Solutions of various metal ions (4.5 μL, 20 mM, 30 eq.) including Na^+, K^+, Ag^+, Mg^{2+}, Hg^{2+}, Pb^{2+}, Ca^{2+}, Cd^{2+}, Co^{2+}, Cu^{2+}, Mn^{2+}, Ni^{2+}, Zn^{2+}, Fe^{2+}, Fe^{3+}, Al^{3+}, Cr^{3+}, and Ga^{3+} were added to each **1** solution (3 mL, 1 μM in bis–tris solutions). $Ga(NO_3)_3$ aqueous solutions (4.5 μL, 20 mM, 30 eq.) were then added to the above solutions. After mixing for 5 min, fluorescence spectra were recorded at room temperature.

^1H NMR titration

NMR samples of sensor **1** (3.02 mg, 0.01 mmol) were dissolved in DMSO-d_6 (500 μL), and different amounts of $Ga(NO_3)_3$ (0–0.5 eq.) were added to each sample. After the mixtures were mixed for 30 minutes, ^1H NMR spectroscopy was performed at room temperature.

Theoretical calculation

The structures of **1** and **1–Ga^{3+}** were fully optimized by DFT calculations using the Gaussian 09 program.[55] The B3LYP functional adopted the 6-31G basis set for H, C, N, O, and S atoms and Lanl2DZ basis set for Ga atoms. The input files were generated using GaussView 6.0 (scaling radii of 75%, isovalue of 0.05). GaussSum 3.0 (ref. 56) was adopted to calculate the contribution of molecular orbitals (MO) in electronic transitions and the theoretical absorption spectrum.

Fluorescent test strips

In order to facilitate rapid detection and analysis, fluorescent test strips for Ga^{3+} detection were developed. A series of rectangle test strips were prepared by adding 10 μL of 10 μM sensor

1 solution and then dried to make Ga^{3+} test strips. Following this, 10 μL 10 μM different metal ions (Na^+, K^+, Ag^+, Mg^{2+}, Hg^{2+}, Pb^{2+}, Ca^{2+}, Cd^{2+}, Co^{2+}, Cu^{2+}, Mn^{2+}, Ni^{2+}, Zn^{2+}, Fe^{2+}, Fe^{3+}, Al^{3+}, Cr^{3+}, and Ga^{3+}) were added to each test strip.
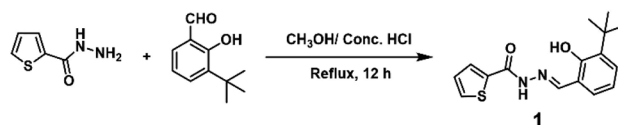
Crystallographic data collection and refinement

A suitable single crystal with a size of 0.3 × 0.2 × 0.1 mm for sensor **1** (CCDC number: 2064800) was selected for single-crystal X-ray diffraction analysis. Data collection was conducted using a Bruker-AXS CCD area detector with graphite monochromatic MoKα ($\lambda = 0.71073$ Å) radiation in the ω scan mode at 296(2) K. Unit-cell parameters were determined by automatic centering of the reflections. The diffraction data were corrected for Lorentz and polarization effects and absorption (empirically from ψ scan data). Using Olex2-1.3,[57] the structure was solved using the SHELXT[58] structure solution program by Intrinsic Phasing and refined using the SHELXL[59] refinement package by least squares minimization. The relevant crystallographic data for **1** are presented in Table 1, and the selected bond lengths and angles are given in Tables S1 and S2, ESI.†

Results and discussion

Synthesis and structural characterization of 1

As shown in Scheme 1, **1** was synthesized by direct condensation of 3-(*tert*-butyl)-2-hydroxybenzaldehyde and thiophene-2-carbohydrazide with a 98.6% yield in a methanol solution and characterized by ^{1}H NMR, ^{13}C NMR, and ESI-MS spectra (see ESI, Fig. S1–S3†). Sensor **1** has good solubility in common organic solvents such as methanol, ethanol, DMF, and DMSO, and slight solubility in water. The single crystal of **1** was achieved by slowly evaporating the solvent (MeOH : MeCN = 4 : 1, v/v) at room temperature. The single-crystal data (Fig. 1, Table 1)

Table 1 Crystallographic details for sensor **1**

Identification code	**1**
Empirical formula	$C_{16}H_{18}N_2O_2S$
Formula weight	302.38
Temperature/K	296.15
Crystal system, space group	Monoclinic, $P2_1/c$
Unit cell dimensions	$a = 19.277(4)$ Å, $\alpha = 90°$
	$b = 9.640(2)$ Å, $\beta = 81.711(7)°$
	$c = 8.8871(18)$ Å, $\gamma = 90°$
Volume/Å^3	1634.2(6)
Z, ρ_{calc} g cm^{-3}	4, 1.229
μ/mm^{-1}, $F(000)$	0.204, 640.0
Crystal size/mm^3	0.3 × 0.2 × 0.1
Radiation	Mo Kα ($\lambda = 0.71073$)
2θ range for data collection/°	4.27 to 46.184
Index ranges	$-21 \leq h \leq 21$, $-10 \leq k \leq 10$, $-9 \leq l \leq 9$
Reflections collected	12 926
Independent reflections	2295 [$R_{int} = 0.0377$, $R_{sigma} = 0.0283$]
Data/restraints/parameters	2295/0/194
Goodness-of-fit on F^2	1.038
Final R indexes [$I \geq 2\sigma(I)$]	$R_1 = 0.0567$, w$R_2 = 0.1576$
Final R indexes [all data]	$R_1 = 0.0824$, w$R_2 = 0.1782$
Largest diff. peak/hole/e Å^{-3}	0.39/−0.41

Scheme 1 Synthesis route of **1**.

of **1** were collected using an X-ray single-crystal diffractometer and solved using the Olex2-1.3 program.[55] As shown in Fig. 1a, there is an intra-molecular H-bonding (O2–H2···N2, 1.87 Å, 2.601 Å, 148.1°) between the hydroxyl proton and the adjacent imine nitrogen, which can reduce the molecular flexibility. However, the rotation of the N–N single bond makes the thiophene ring and the salicylaldehyde part form a dihedral angle with 24.52° (Fig. 1e). Clearly, the molecular rotation of **1** in the solution will be more significant than that in the crystallized state, which contributes to the difference in the solution and solid-state fluorescence emissions (see ESI, Fig. S4†). The molecules of **1** were connected by a strong intermolecular hydrogen bond N1–H1/O1 (1.992 Å, 2.815 Å, 159.9°) into a one-dimensional chain. Then, these 1D chains are stacked by van der Waals interactions along 2D and 3D directions in the crystal lattice (Fig. 1b–d).

UV-vis absorption studies

The UV-vis absorption spectrum of sensors is an essential photophysical property for the investigation on sensing property. The absorption spectrum of **1** and **1**–Ga^{3+} in a bis–tris buffer solution (about 0.3% $DMSO/H_2O$) was recorded at room temperature. As shown in ESI, Fig. S5,† the UV-vis spectrum of **1** shows two prominent absorption bands at 306 nm and 338 nm, corresponding to π–π* and n–π* transitions, respectively. **1**–Ga^{3+} shows two notable absorption bands at 315 and 405 nm.
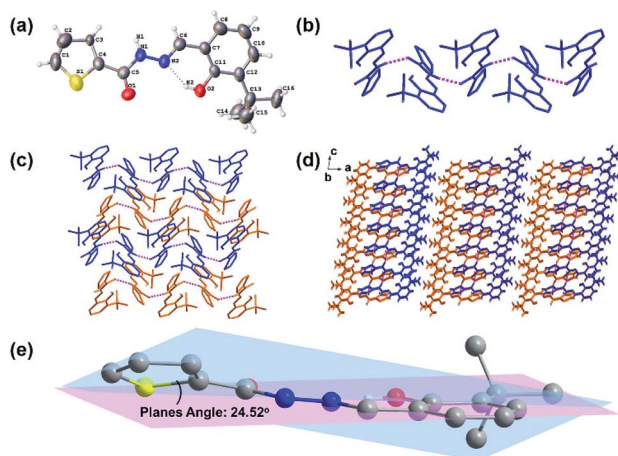

Fig. 1 Views of sensor **1**: (a) ORTEP representation showing the crystal structure of **1** with 30% thermal ellipsoid probability; (b) the 1D belt linked by H-bondings (N1–H1···O1, 1.992 Å, 2.815 Å, 159.9°); (c) the 2D and (d) 3D structures formed by van der Waals interactions viewed down from the *b* axis (hydrogen atoms without forming H-bonds are omitted for clarity); and (e) dihedral angle of the molecule of **1**.

The maximum absorption peaks of sensor **1** and **1–Ga³⁺** are 338 and 404 nm, respectively. The binding ability of **1** and Ga³⁺ ion was initially studied by UV-vis titration analysis. As shown in Fig. 2a, upon the addition of Ga³⁺ (0–0.5 eq.), the absorption peaks near 306 and 338 nm of **1** gradually decreased. **1–Ga³⁺** has a new absorption band near 404 nm, which are attributed to the π–π* transition of the thiophene unit and the charge transfer transition in the Ga³⁺ complex. As a result, the maximum absorption peak shifted from 338 nm to 404 nm. Two clear isosbestic points (266 and 354 nm) indicates the formation of complex **1–Ga³⁺** between **1** and Ga³⁺. As shown in Fig. 2b, S6 and S7,† the calculated spectrum shows the calculated maximum absorption peaks of **1** and **1–Ga³⁺** to be 348 and 406 nm (a similar red-shift occurs from **1** to **1–Ga³⁺**). The calculated results are consistent with the experimental results, validating the experimental results.

In order to determine the stoichiometry of **1** towards Ga³⁺, we carried out Job's plot in a bis–tris buffer solution (Fig. 2c). According to Job's plot, when the abscissa value is 0.33, the fluorescence intensity is the strongest, which is equivalent to the sensor-to-ion ratio of 2 : 1. The ESI mass spectrum was regarded as the direct evidence to determine the stoichiometry between metal ions and sensors (Fig. 2d). Furthermore, the ESI mass spectrum of **1–Ga³⁺** in CH₃OH was achieved. The ESI-MS mass spectrum peak at m/z 671.1275, corresponding to $[2 \cdot \mathbf{1} + \mathbf{Ga^{3+}} - 2H^+]^+$ (calcd = 671.1272), can be observed when an excess amount of Ga³⁺ was added to **1**, suggesting a 2 : 1 ligand–Ga³⁺ binding stoichiometry (Fig. 2d). This result is consistent with the result of Job's plot.

In order to further study the linear relationship between **1** and Ga³⁺, the absorption intensity graph of **1** *versus* Ga³⁺ concentrations was achieved (see ESI, Fig. S8†). The association constants (K_a) of **1–Ga³⁺** complex were calculated to be 8.5×10^3 through Benesi–Hildebrand expression (see ESI, Fig. S9†). In practical applications, LOD and LOQ are important parameters to measure the detection ability of a sensor. The calibration curve was plotted as **1** *versus* Ga³⁺ concentrations (0–5 μM), which was found linear [$R^2 = 0.9951$, SD = 0.0002, $n = 11$, and $m = 0.0104$]. The LOD and LOQ of sensor **1** towards Ga³⁺ were calculated according to the eqn (1) and (2),[28] and were found as 58 nM, and 192 nM, respectively. In eqn (1) and (2), m refers to the slope of the calibration curve, and SD is the standard deviation of the absorption intensity of different Ga³⁺ concentrations. The comparative analysis of **1** with previously reported Ga³⁺ sensors is shown in Table S3, ESI.† It can be seen from the comparison results that sensor **1** has the following advantages: easy synthesis, determined structure, water solubility, lower LOD, and specific recognition of Ga³⁺.

$$\mathrm{LOD} = 3\frac{\mathrm{SD}}{m} \qquad (1)$$

$$\mathrm{LOQ} = 10\frac{\mathrm{SD}}{m} \qquad (2)$$

¹H NMR titrations

In order to clarify the binding mode and coordination position of Ga³⁺ to **1**, and better explain the detection mechanism, ¹H NMR titration was performed by adding different amounts of Ga³⁺ (0–0.5 eq.) to sensor **1**. The chemical shifts of H atoms of sensor **1** were assigned in the ¹H NMR spectrum, as shown in Fig. 3. The N–H (H4) chemical shift is at 12.32 ppm, and O–H (H₉) chemical shift is at 12.26 ppm. After the addition of Ga³⁺ to sensor **1**, the ¹H NMR spectrum significantly changed (Fig. 3). The chemical shift signals of H₄ and H₉ gradually weakened. After the addition amount of Ga³⁺ reached 0.5 eq., chemical shift signals disappear entirely. These results can also verify that the binding stoichiometry of **1** to Ga³⁺ was 2 : 1. The disappearance of the strong N–H (H₄) and O–H (H₉) peaks of phenol-OH suggests that H4 participating enol tautomeric carbonyl and H9 involving interaction between the phenolic hydroxyl group and Ga³⁺. All changes in the ¹H NMR spectrum suggest that two molecular of sensor **1** are coordinated with one Ga³⁺ through two O atoms of the carbonyl group, two azomethine-N atoms, and two phenolic-OH O atoms.
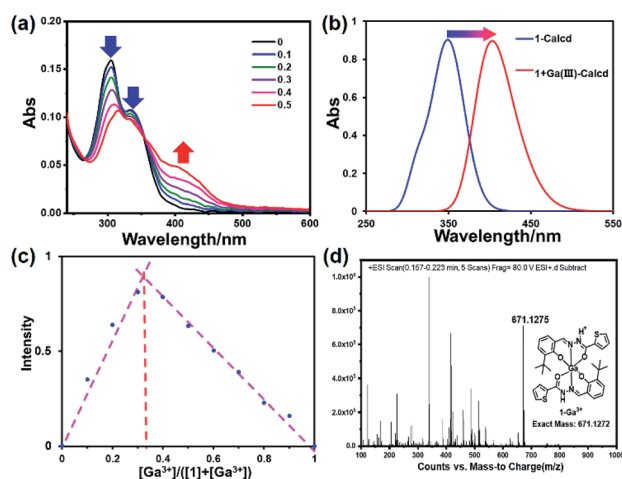

Fig. 2 (a) Absorption spectra of **1** (10 μM) upon the addition of Ga³⁺ (0–0.5 eq.) in 0.3% DMSO/bis–tris buffer solution. (b) Theoretical calculated UV-vis absorption spectrum of **1** and **1–Ga³⁺**. (c) Job's plot for determining the stoichiometry of **1** and Ga³⁺ in 0.03% DMSO/bis–tris buffer solution. (d) ESI-MS spectrum of **1–Ga³⁺**.

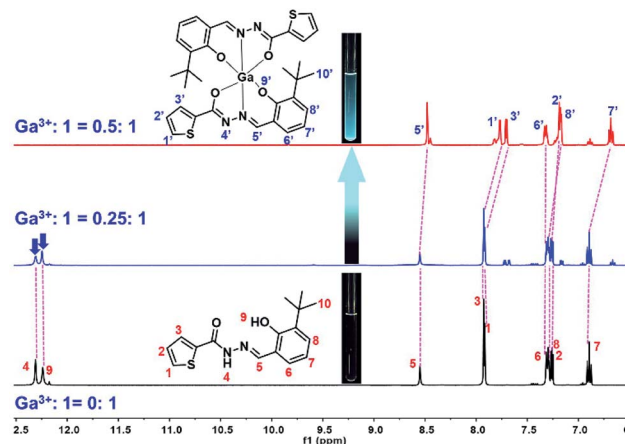**Fig. 3** ¹H NMR titration of **1** upon the addition of Ga³⁺ (0–0.5 eq.) in DMSO-d_6 (inset: photograph of **1** and **1–Ga³⁺** in the NMR tube under the irradiation of a 365 nm UV lamp).

Fluorescence studies

The fluorescence spectrum of **1** in the presence of various metal ions (Na$^+$, K$^+$, Ag$^+$, Mg^{2+}, Hg^{2+}, Pb^{2+}, Ca^{2+}, Cd^{2+}, Co^{2+}, Cu^{2+}, Mn^{2+}, Ni^{2+}, Zn^{2+}, Fe^{2+}, Fe^{3+}, Al^{3+}, Cr^{3+}, and Ga^{3+}) was studied (Fig. 4). The fluorescence spectra of all these ions were recorded under the same condition. As shown in Fig. 4a and d, apparent spectral changes were observed only in the presence of Ga^{3+}. In contrast, treatment with other metal ions resulted in no apparent phenomenon, evidencing that **1** is a highly selective and specific sensor for Ga^{3+} over other metal ions. In order to study the anti-interference ability during the detection process of sensor **1**, we conducted competitive ion experiments (Fig. 4e). The operation of the competitive ion experiments is to add other metal ions to the **1–Ga^{3+}** solution, and then test the fluorescence intensity of the mixed ion solution. We can observe that the fluorescence intensity of complex **1–Ga^{3+}** was not significantly affected by most of the coexistent metal ions. Therefore, sensor **1** can be used as an effective fluorescent sensor for Ga^{3+} in the presence of most competing metal ions. In order to observe and compare the effect of fluorescence changes more intuitively, we conducted experiments on sensor **1** with different metal ions in a series of sample bottles (Fig. 4c). The results indicate that the fluorescence in most sample bottles has almost no change, except for those containing Ga^{3+} under the irradiation of an UV lamp. Compared with **1**, the fluorescence intensity of its Ga^{3+} complex changed dramatically with a strong blue-green fluorescence emission (see ESI, Fig. S10†). However, no obvious fluorescence colour and intensity changed when other metal ions were added to **1**

(Fig. 4c). Moreover, because Ga^{3+} and Al^{3+} have similar chemical properties, the task of distinguishing them is a well-known challenge.[60] Therefore, we also carried out UV titration experiments on Al^{3+} with sensor **1** (see ESI, Fig. S11†). The result indicates that with the addition of Al^{3+}, even if the amount reaches 30 equivalents, the wavelength of the absorption spectrum does not change significantly. There is also no equivalent absorption point in the titration curve, which is completely different from the titration result of sensor **1** by Ga^{3+}. Therefore, sensor **1** has high selectivity and specificity for recognizing Ga^{3+}.

In order to conduct a more in-depth study of sensor **1** and Ga^{3+}, we performed fluorescence titration experiments on the addition of Ga^{3+} towards sensor **1** (Fig. 4b). As shown in Fig. 4b, free sensor **1** showed very weak fluorescence emission in the bis–tris buffer solution, which may be caused by the ESIPT effect. Upon the addition of Ga^{3+} ions (0–0.5 eq.), the fluorescence intensity of **1–Ga^{3+}** increases linearly with a significant enhancement at 480 nm. The quantitative experiment of fluorescence titration can also prove that the probe-to-ion binding ratio is 2 : 1. The fluorescence quantum yields of **1** and **1–Ga^{3+}** (1 μM) are 0.012 and 0.28, respectively. Quantum yield was improved more than 20 times after the binding process.

The time-dependent fluorescence response spectrum shows that it takes 30 seconds to reach the saturated steady-state fluorescence intensity (see ESI, Fig. S12†). The pH effect was also verified because it is an important indicator of sensor applications (see ESI, Fig. S13†). The fluorescence intensity of free sensor **1** remains almost unchanged in the range of pH = 3–12. However, in the presence of Ga^{3+}, the fluorescence ratio showed a strong change in the pH range of 4–8, strongly indicating that sensor **1** is suitable for monitoring Ga^{3+} under physiological conditions.

Theoretical calculation

The possible binding mode of sensor **1** and Ga^{3+} was verified by Job's plot, ESI-MS, and ^{1}H NMR titration, that is, sensor **1** and Ga^{3+} were connected through a 2 : 1 coordination ratio. The possible connection mode is that one gallium atom is coordinated with two imino N atoms, two phenolic hydroxyl O atoms, and two carbonyl O atoms of two **1** ligands. The DFT calculation was performed to optimize the possible molecular structure of **1–Ga^{3+}** based on B3LYP/6-31G(d) (Fig. 5). The TD-DFT calculation was operated to study the spectral change behavior from **1** to **1–Ga^{3+}**. As shown in the calculated results, the highest occupied molecular orbital (HOMO) of **1** is mainly located within the benzene ring, acylhydrazine, and Schiff base framework. The lowest unoccupied molecular orbital (LUMO) of **1** is distributed in the π-conjugated skeleton of the intact molecule. The HOMO of **1–Ga^{3+}** is also located within the benzene ring, acylhydrazine, and Schiff base framework. The LUMO of **1–Ga^{3+}** is also distributed in the whole-molecule π-conjugated skeleton. The HOMO and LUMO energy levels of **1** are −5.69 eV and −1.78 eV. In addition, the HOMO and LUMO energy levels of **1–Ga^{3+}** are −2.26 eV and 1.10 eV (Fig. 5, Tables S4–S6†). Therefore, we can obtain the HOMO–LUMO energy gap (E_{gap}) values of **1** and **1–Ga^{3+}** at 3.91 and 3.36 eV through the formula $E_{gap} =$
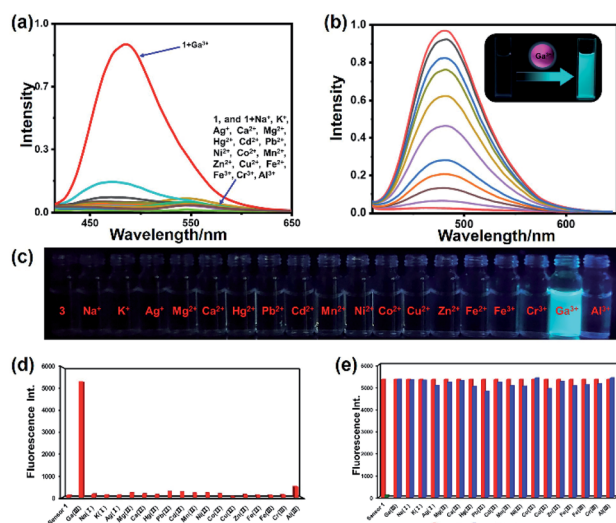

Fig. 4 (a) Fluorescence spectra of **1** (1 μM) with metal ions (30 μM) (Na$^+$, K$^+$, Ag$^+$, Mg^{2+}, Ca^{2+}, Hg^{2+}, Pb^{2+}, Cd^{2+}, Mn^{2+}, Ni^{2+}, Co^{2+}, Cu^{2+}, Zn^{2+}, Fe^{2+}, Fe^{3+}, Cr^{3+}, Al^{3+} and Ga^{3+}). (b) Fluorescence spectra of **1** (1 μM) upon addition of Ga^{3+} in 0.03% DMSO/tris−bis buffer solution (inset: photo of **1** and its Ga^{3+} complex solution under 365 nm UV lamp irradiation). (c) Fluorescence photo of **1** (10 μM) and **1** with metal ions (10 μM) under the irradiation of a 365 nm UV lamp. (d) Fluorescence intensity of **1** (1 μM) with different metal ions. (e) Competitive experiments of **1–Ga^{3+}** toward other metal ions.
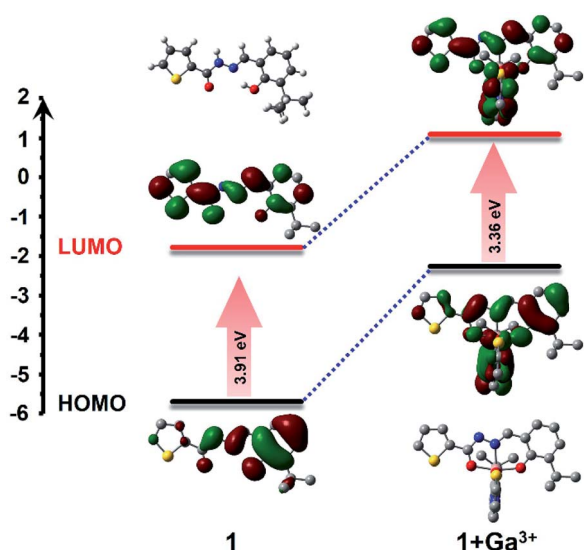
Fig. 5 Optimized molecular structure and HOMO and LUMO orbital levels and energy gap of **1** and **1 + Ga³⁺**, calculated with DFT at the B3LYP/6-31G(d) level using Gaussian 09.

Table 2 Detection of Ga³⁺ in water samples[a]

Sample	Ga³⁺ added (μM)	Ga³⁺ found (μM)	Recovery (%)	RSD% (n = 3)
Drinking water	0	0	—	—
	1.0[b]	0.986	98.6	0.33
Tap water	0	0	—	—
	1.0[c]	0.972	97.2	0.41

[a] Conditions: the concentration of sensor **1** is 1 μM in bis–tris buffer solution. [b] 3 mM Ga³⁺ was added artificially to the drinking water sample to reach 1.0 μM concentration. [c] 3 mM Ga³⁺ was added artificially to the tap water sample to reach 1.0 μM concentration.

$E_{\text{LUMO}} - E_{\text{HOMO}}$. The energy gap value of **1–Ga³⁺** is lower than that of **1**. The E_{gap} decreased significantly from **1** to **1–Ga³⁺**, indicating that E_{gap} become narrower during the combination process, which means that it takes less energy to excite **1–Ga³⁺** than **1**. Thus, a red-shift in the absorption spectrum occurred from **1** to **1–Ga³⁺**. The E_{gap} gradually becomes narrower from **1** to **1–Ga³⁺**, which means the maximum absorption wavelength gradually becomes more extensive and coincides with the experimental results.

Possible sensing mechanism of 1

From the single-crystal structure of **1** (Fig. 1a) and the optimized structure diagram of **1** and **1–Ga³⁺** (see ESI, Fig. S14 and S15†), we can observe that the flexibility of **1** was restricted through the crystallization and coordination to Ga³⁺. Due to the existence of intramolecular hydrogen bonds, there is the ESIPT effect in the molecule, which can make the molecular fluorescence very weak. The solid-state fluorescence spectrum was conducted using bulky crystallized samples (see ESI, Fig. S4 and S16†), which is stronger than the solution fluorescence emission, as we expect. The molecular charge distribution was also changed after the coordination with Ga³⁺, which is favorable to

fluorescence emission in the energy level. Therefore, the possible sensing mechanism of **1** was proposed, according to which the interaction of **1** and Ga³⁺ brings about intramolecular hydrogen bond (O–H···N) cleavage and enol interconversion of the carbonyl group, which inhibits the ESIPT and PET effects (Fig. 6). As a result, **1–Ga³⁺** showed fluorescence enhancement up to 50 folds.

Application of Ga³⁺ test strips and determination in water samples

In order to explore the practical application of sensor **1** and make it easily and conveniently applied in our daily lives, we developed test strips based on sensor **1**. A series of 3 mM sensor **1** solutions were dropped onto the filter paper strips and dried to obtain test strips. Then, metal ion solutions were added dropwise onto the strips. After a few seconds, under a 365 nm UV lamp, we can observe that the test strip with Ga³⁺ emitted strong blue-green fluorescence (Fig. 6b). However, the fluorescence of test strips without Ga³⁺ ions was almost unchanged. This result indicates that simple and easy-prepared test strips can detect Ga³⁺. As shown in Table 2, we conducted the practical application of sensor **1** in drinking water and tap water. The experimental results of both water samples showed appropriate recovery rates. We also calculated the relative standard deviation (RSD) of the experiment. These results indicate that **1** can be used as a useful sensor for determining the Ga³⁺ content in actual water samples.

Conclusions

In summary, we have synthesized and characterized a novel sensor, **1**, based on the thiophene acylhydrazone Schiff base. Sensor **1** has outstanding highly selective and specific "turn-on" fluorescence recognition ability for Ga³⁺ detection in aqueous solutions. The interaction of sensor **1** with Ga³⁺ has been investigated based on ESI-MS spectrometry, ¹H NMR titration, fluorescence emission, and theoretical calculations. The possible sensing mechanism was proposed with the ESIPT effect. The LOD of **1** towards Ga³⁺ was found to reach a 10^{-8} M level in an aqueous solution. Moreover, highly selective test strips based on sensor **1** have been developed for Ga³⁺ detection. Sensor **1** was also used to detect Ga³⁺ concentration in
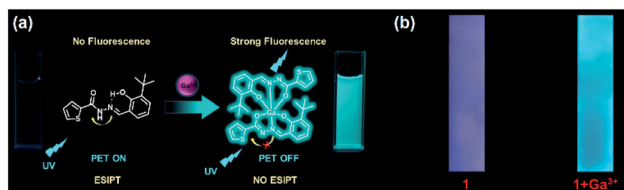

Fig. 6 (a) Proposed sensing mechanism of sensor **1** to Ga³⁺. (b) Photograph of test paper strips of **1** and **1 + Ga³⁺** under the irradiation of a 365 nm UV lamp.

actual water samples, and a considerable recovery rate was obtained. Based on the results, we believe that this work will contribute to the development and application in gallium detection fields.

Conflicts of interest

There are no conflicts to declare.

Acknowledgements

Notes and references

1 L. R. Bernstein, *Pharmacol. Rev.*, 1998, **50**, 665.
2 C. Lim, M. An, H. Seo, J. H. Huh, A. Pandith, A. Helal and H. S. Kim, *Sens. Actuators, B*, 2017, **241**, 789.
3 D. Yun, J. M. Jung and C. Kim, *Inorg. Chim. Acta*, 2018, **479**, 154.
4 H. Dong, H. Zhu, Q. Meng, X. Gong and W. Hu, *Chem. Soc. Rev.*, 2012, **41**, 1754.
5 J. Yoon, S. Jo, I. S. Chun, I. Jung, H. S. Kim, M. Meitl, E. Menard, X. Li, J. J. Coleman, U. Paik and J. A. Rogers, *Nature*, 2010, **465**, 329.
6 H. M. Kim, Y. H. Cho, H. Lee, S. I. Kim, S. R. Ryu, D. Y. Kim, T. W. Kang and K. S. Chung, *Nano Lett.*, 2004, **4**, 1059.
7 R. Trotta, P. Atkinson, J. D. Plumhof, E. Zallo, R. O. Rezaev, S. Kumar, S. Baunack, J. R. Schroter, A. Rastelli and O. G. Schmidt, *Adv. Mater.*, 2012, **24**, 2668.
8 J. M. Kikkawa and D. D. Awschalom, *Nature*, 1999, **397**, 139–141.
9 J. Goldberger, R. He, Y. Zhang, S. Lee, H. Yan, H. J. Choi and P. Yang, *Nature*, 2003, **422**, 599.
10 A. Kumar, J. Y. Lee and H. S. Kim, *Sens. Actuators, B*, 2017, **239**, 85.
11 F. Wang, T. Gao, Q. Zhang, Z. Y. Hu, B. Jin, L. Li, X. Zhou, H. Li, G. V. Tendeloo and T. Zhai, *Adv. Mater.*, 2018, e1806306.
12 S. Crunkhorn, *Nat. Rev. Drug Discovery*, 2018, **17**, 786.
13 M. M. Berggren, L. A. Burns, R. T. Abraham and G. Powis, *Cancer Res.*, 1993, **53**, 1862.
14 D. Kara, A. Fisher, M. Foulkes and S. Hill, *Spectrochim. Acta, Part A*, 2010, **75**, 361.
15 H. J. Jang, J. H. Kang, D. Yun and C. Kim, *Photochem. Photobiol. Sci.*, 2018, **17**, 1247.
16 V. K. Gupta, A. J. Hamdan and M. K. Pal, *Anal. Chim. Acta*, 2010, **673**, 139.
17 X. He, C. Wu, Y. Qian, Y. Li, F. Ding, Z. Zhou and J. Shen, *Talanta*, 2019, **205**, 120118.
18 X. He, C. Wu, Y. Qian, Y. Li, L. Zhang, F. Ding and J. Shen, *Analyst*, 2019, **144**, 3807.
19 X. He, W. Xiong, C. Xu, J. Fan, Y. Qian, J. Wen and J. Shen, *Dyes Pigm.*, 2020, **174**, 108059.
20 A. Kumar and P. S. Chae, *Anal. Chim. Acta*, 2017, **958**, 38.
21 F. Cai, F. Xia, Y. Guo, W. Zhu, B. Fu, X. Liang, S. Wang, Z. Cai and H. Xu, *New J. Chem.*, 2019, **43**, 18012.
22 V. Kumar, P. Kumar, S. Kumar, D. Singhal and R. Gupta, *Inorg. Chem.*, 2019, **58**, 10364.
23 L. Liu, A. Wang, G. Wang, J. Li and Y. Zhou, *Sens. Actuators, B*, 2015, **215**, 388.
24 H. Tavallali, P. Vahdati and E. Shaabanpur, *Sens. Actuators, B*, 2011, **159**, 154.
25 Z. Wang, Y. Zhang, J. Yin, M. Li, H. Luo, Y. Yang, X. Xu, Q. Yong and S. Wang, *Sens. Actuators, B*, 2020, **320**, 128249.
26 X. Zhang, Y. Jiang and N. Xiao, *Chem. Commun.*, 2018, **54**, 12812.
27 T. A. Sheikh, M. N. Arshad, A. M. Asiri and M. M. Rahman, *New J. Chem.*, 2018, **42**, 13589.
28 M. M. Hussain, A. M. Asiri, M. N. Arshad and M. M. Rahman, *New J. Chem.*, 2018, **42**, 1169.
29 H. J. Jang, J. H. Kang, D. Yun and C. Kim, *Photochem. Photobiol. Sci.*, 2018, **17**, 1247.
30 Y. W. Wang, S. B. Liu, W. J. Ling and Y. Peng, *Chem. Commun.*, 2016, **52**, 827.
31 J. Kimura, H. Yamada, H. Ogura, T. Yajima and T. Fukushima, *Anal. Chim. Acta*, 2009, **635**, 207.
32 J. Y. Noh, S. Kim, I. H. Hwang, G. Y. Lee, J. S. Kang, H. Kim, J. Min, S. Park, C. Kim and J. Kim, *Dyes Pigm.*, 2013, **99**, 1016.
33 X. He, W. Xiong, C. Xu, J. Fan, Y. Qian, J. Wen and J. Shen, *Dyes Pigm.*, 2020, **174**, 108059.
34 L. Guo, M. Tian, Z. Zhang, Q. Lu, Z. Liu, G. Niu and X. Yu, *J. Am. Chem. Soc.*, 2021, **143**, 3169.
35 J. Kong, C. He, X. Zhang, Q. Meng and C. Duan, *Dyes Pigm.*, 2014, **101**, 254.
36 S. Sharma, G. Dubey, B. S. Sran, P. V. Bharatam and G. Hundal, *ACS Omega*, 2019, **4**, 18520.
37 F. Shi, S. Cui, H. Liu and S. Pu, *Dyes Pigm.*, 2020, **173**, 107914.
38 Y. Tang, Y. Ma, J. Yin and W. Lin, *Chem. Soc. Rev.*, 2019, **48**, 4036.
39 H. Dong, M. Luo, S. Wang and X. Ma, *Dyes Pigm.*, 2017, **139**, 118.
40 M. Jiang, X. Gu, J. W. Y. Lam, Y. Zhang, R. T. K. Kwok, K. S. Wong and B. Z. Tang, *Chem. Sci.*, 2017, **8**, 5440.
41 Z. Li, M. Ren, L. Wang, L. Dai and W. Lin, *Sens. Actuators, B*, 2020, **307**, 127643.
42 W. Fu, C. Yan, Z. Guo, J. Zhang, H. Zhang, H. Tian and W. H. Zhu, *J. Am. Chem. Soc.*, 2019, **141**, 3171.
43 Y. Jiao, L. Zhang, X. Gao, W. Si and C. Duan, *Angew. Chem., Int. Ed.*, 2020, **59**, 6021.
44 X. Li, X. Gao, W. Shi and H. Ma, *Chem. Rev.*, 2014, **114**, 590.
45 K. Boonkitpatarakul, J. Wang, N. Niamnont, B. Liu and L. Mcdonald, *ACS Sens.*, 2015, **1**, 144.
46 S. M. Hwang, M. S. Kim, M. Lee and M. H. Lim, *New J. Chem.*, 2017, **41**, 15590.
47 H. Y. Jeong, S. Y. Lee, J. Han and M. H. Lim, *Tetrahedron*, 2017, **73**, 2690.
48 C. Balakrishnan, M. A. Neelakantan and S. Banerjee, *Sens. Actuators, B*, 2017, **253**, 1012.
49 J. Fu, B. Li, H. Mei, Y. Chang and K. Xu, *Spectrochim. Acta, Part A*, 2019, **227**, 117678.

50 J. Lian, Q. Xu, Y. Wang and F. Meng, *Front. Chem.*, 2020, **8**, 1016.

51 L. Hao, Q. Qiu, W. Wang, L. Gu and H. Li, *Chin. J. Chem.*, 2016, **34**, 1109.

52 J. B. Song, P. Wang, L. Yan, L. Hao, M. A. Khan, G. L. Liu and H. Li, *Dalton Trans.*, 2020, **49**, 4358.

53 P. Wang, L. Liu, F. Meng, M. A. Khan and H. Li, *Front. Chem.*, 2020, **8**, 1006.

54 A. Han, H. Su, G. Xu, M. A. Khan and H. Li, *RSC Adv.*, 2020, **10**, 23372.

55 M. J. Frisch, G. W. Trucks, H. B. Schlegel, G. E. Scuseria, M. A. Robb, J. R. Cheeseman, G. Scalmani, V. Barone, B. Mennucci, G. A. Petersson, H. Nakatsuji, M. Caricato, X. Li, H. P. Hratchian, A. F. Izmaylov, J. Bloino, G. Zheng, J. L. Sonnenberg, M. Hada, M. Ehara, K. Toyota, R. Fukuda, J. Hasegawa, M. Ishida, T. Nakajima, Y. Honda, O. Kitao, H. Nakai, T. Vreven, J. A. Montgomery Jr, J. E. Peralta, F. Ogliaro, M. Bearpark, J. J. Heyd, E. Brothers, K. N. Kudin, V. N. Staroverov, R. Kobayashi, J. Normand, K. Raghavachari, A. Rendell, J. C. Burant, S. S. Iyengar, J. Tomasi, M. Cossi, N. Rega, J. M. Millam, M. Klene, J. E. Knox, J. B. Cross, V. Bakken, C. Adamo, J. Jaramillo, R. Gomperts, R. E. Stratmann, O. Yazyev, A. J. Austin, R. Cammi, C. Pomelli, J. W. Ochterski, R. L. Martin, K. Morokuma, V. G. Zakrzewski, G. A. Voth, P. Salvador, J. J. Dannenberg, S. Dapprich, A. D. Daniels, O. Farkas, J. B. Foresman, J. V. Ortiz, J. Cioslowski, and D. J. Fox, *Gaussian 09, Revision. D.01*, Gaussian, Inc., Wallingford CT, 2009.

56 N. M. O'Boyle, A. L. Tenderholt and K. M. Langner, *J. Comput. Chem.*, 2008, **29**, 839–845.

57 O. V. Dolomanov, L. J. Bourhis, R. J. Gildea, J. A. Howard and H. Puschmann, *J. Appl. Crystallogr.*, 2009, **42**, 339.

58 G. M. Sheldrick, *Acta Crystallogr., Sect. A: Found. Adv.*, 2015, **71**, 3.

59 G. M. Sheldrick, *Acta Crystallogr., Sect. C: Struct. Chem.*, 2015, **71**, 3.

60 S. Y. Lee, K. H. Bok, T. G. Jo, S. Y. Kim and C. Kim, *Inorg. Chim. Acta*, 2017, **461**, 127.